Tech Science Press

Fast Force Loading Disrupts Molecular Binding Stability in Human and Mouse Cell Adhesions

Yunfeng Chen[1,2,3,†,*], Jiexi Liao[4,†], Zhou Yuan[1], Kaitao Li[4], Baoyu Liu[4], Lining Arnold Ju[4,5,6] and Cheng Zhu[1,2,4,*]

[1]Woodruff School of Mechanical Engineering, Georgia Institute of Technology, Atlanta, Georgia, 30332, USA.

[2]Petit Institute for Bioengineering and Biosciences, Georgia Institute of Technology, Atlanta, Georgia, 30332, USA.

[3]Department of Molecular Medicine, MERU-Roon Research Center on Vascular Biology, The Scripps Research Institute, La Jolla, California, 92037, USA.

[4]Coulter Department of Biomedical Engineering, Georgia Institute of Technology, Atlanta, Georgia, 30332, USA.

[5]Heart Research Institute, University of Sydney, Camperdown, NSW 2006, Australia.

[6]Charles Perkins Centre, tUniversity of Sydney, Camperdown, NSW 2006, Australia.

[†]These authors contributed equally.

[*]Correspondence Authors: Yunfeng Chen. Email: cheny@scripps.edu; Cheng Zhu. Email: cheng.zhu@bme.gatech.edu.

Abstract: Force plays critical roles in cell adhesion and mechano-signaling, partially by regulating the dissociation rate, i.e., off-rate, of receptor-ligand bonds. However, the mechanism of such regulation still remains elusive. As a controversial topic of the field, when measuring the "off-rate *vs.* force" relation of the same molecular system, different dynamic force spectroscopy (DFS) assays (namely, force-clamp and force-ramp assays) often yield contradictive results. Such discrepancies hurdled our further understanding of molecular binding, and casted doubt on the existing theoretical models. In this work, we used a live-cell DFS technique, biomembrane force probe, to measure the single-bond dissociation in three receptor-ligand systems which respectively have important functions in vascular and immune systems: human platelet GPIbα-VWF, mouse T cell receptor-OVA peptide:MHC, and mouse platelet integrin $\alpha_{IIb}\beta_3$-fibrinogen. Using force-clamp and force-ramp assays in parallel, we identified that the force loading disrupted the stability of molecular bonds in a rate-dependent manner. This disruptive effect was achieved by the transitioning of bonds between two dissociation states: faster force loading induces more bonds to adopt the fast-dissociating state (and less to adopt the slow-dissociating state). Based on this mechanism, a new biophysical model of bond dissociation was established which took into account the effects of both force magnitude and loading rate. Remarkably, this model reconciled the results from the two assays in all three molecular systems under study. Our discoveries provided a new paradigm for understanding how force regulates receptor-ligand interactions and a guideline for the proper use of DFS technologies. Furthermore, our work highlighted the opportunity of using different DFS assays to answer specific biological questions in the field of cell adhesion and mechano-signaling.

Keywords: Force-regulated molecular binding; dynamic force spectroscopy; biophysical model; cell adhesion and mechano-signaling

1 Introduction

Mechanical force plays a crucial role in cell-cell and cell-substrate communications. Force-regulated molecular interactions initiate many cellular activities such as adhesion, migration, and cytoskeleton restructuring. Dynamic force spectroscopy (DFS) [1] which includes atomic force microscopy (AFM), optical tweezer, and biomembrane force probe (BFP), currently serves as the mainstream technology to

measure force-regulated molecular interactions at the single-molecule level. Combined with concurrent intracellular signaling readouts, DFS technologies enable direct correlation of molecular binding kinetics with mechano-signaling in real-time [2,3,4], demonstrating the importance of molecular binding kinetics on cellular functions.

Off-rate (k_{off}, rate of bond dissociation) is an important attribute of receptor-ligand interaction that reflects bond stability: the higher the off-rate, the less stable the bond. Over the last few decades, two major DFS-based assays have emerged to obtain the k_{off} of single molecular bonds: 1) force-clamp assay directly measures bond lifetimes (the reciprocal of k_{off}) by clamping the bond at a constant force [5]; 2) force-ramp assay derives k_{off} from the rupture force magnitudes by ramping the bond with constant force loading rate [6,7]. Both assays demonstrated k_{off} as a function of force magnitude [5,7-13]. However, as a controversial topic of the field, the "k_{off} vs. force" relations derived from the above two assays were often in discrepancy, despite similar experimental setups/conditions. For instance, a catch bond behavior have been observed in the interactions of P-selectin-PSGL-1 [5], integrin $\alpha_5\beta_1$–fibronectin [10], integrin $\alpha_L\beta_2$-ICAM-1 [8] and integrin $\alpha_4\beta_1$-VCAM-1 [9] using the DFS force-clamp assay, where the bond lifetime increases (and therefore k_{off} decreases) with force within a certain force regime. Yet, analysis of the same biological systems in DFS force-ramp assay resulted in slip bonds, where the k_{off} monotonically increased with force [7,11-13]. Even with the same AFM setup, k_{off} was measured to be different for P-selectin-sPSGL-1 and P-selectin-G1 interactions, not only between force-clamp and -ramp assays, but also within the force-ramp assay amongst different force loading rates [14]. Such discrepancies casted doubt on the general applicability of existing theoretical models assuming k_{off} to be a function of only force magnitude [15-19], and suggested that bond stability can be affected by other attributes of force application as well.

In this work, we measured the binding kinetics of three receptor-ligand systems using the force-clamp and force-ramp assays in parallel, and discovered that fast force loading can disrupt bond stability. By investigating the underlying mechanism, we established a new theoretical model that depicts the regulation of bond dissociation by both force magnitude and loading rate.

2 Methods

2.1 Proteins, Antibodies and Reagents

Recombinant monomeric VWF 1208-A1 (residues A0742-17/21; abbreviated as VWF-A1) [20] was from Zaverio Ruggeri (The Scripps Research Institute, La Jolla, CA). Fibrinogen was purchased from Enzyme Research Laboratories. Recombinant pMHC monomers were from the NIH Tetramer Core Facility at Emory University. Chicken ovalbumin-derived peptide OVA257-264 (SIINFEKL) were synthesized and presented by C-terminally biotinylated mouse MHC class I H2-Kbα3A2 (a mutant of H2-Kb with mouse α3 domain replaced by human HLA-A2).

Antibody 6G1 was a gift from Dr. Michael Berndt (Curtin University, WA, Australia). Streptavidin-maleimide (SA-MAL) and bovine serum albumin (BSA) were from Sigma-Aldrich (St. Louis, MO). MAL-PEG3500-NHS and biotin-PEG3500-NHS were from JenKem (Plano, TX). Borosilicate glass beads were from Distrilab Particle Technology (RC Leusden, The Netherlands). All other reagents were from Sigma-Aldrich unless stated otherwise.

2.2 Blood Collection and Platelet Isolation and Preparation

All procedures involving the collection of blood from healthy human donors were approved by the Institutional Review Board of the Georgia Institute of Technology (protocol number H12354). All human donor blood samples were obtained with written informed consent. Human blood was slowly drawn from the vein of a healthy volunteer to fill in a 3 ml syringe preloaded with 0.43 ml ACD buffer (85 mM sodium citrate, 72.9 mM citric acid anhidrous, 110 mM D-glucose and 70 mM Theophylline, pH 4.6). Whole blood was transferred into a 15 ml tube pre-loaded with apyrase (0.005 U mL^{-1}) and Clexane (20 U mL^{-1}). After resting for 15 min at 37ºC, whole blood was centrifuged at 200 g for 10 min without brake. Platelet-rich plasma was extracted, allowed to rest for 10 min at 37ºC and centrifuged at 1,700 g for another 5 min. The

platelet pellet was resuspended into platelet washing buffer (4.3 mM K_2HPO_4, 4.3 mM Na_2HPO_4, 24.3 mM NaH_2PO_4, 113 mM NaCl, 5.5 mM D-Glucose, 10 mM theophylline and 1% BSA, pH 6.5) pre-added with Clexane (20 U mL^{-1}) and apyrase (0.01 U mL^{-1}), rested for 10 min and centrifuged again at 1,500 g for 5 min. The platelet pellet was resuspended into Hepes-Tyrode buffer (134 mM NaCl, 12 mM $NaHCO_3$, 2.9 mM KCl, 0.34 mM sodium phosphate monobasic, 5 mM HEPES, and 5 mM glucose, 1% BSA, pH 7.4) pre-added with apyrase (0.02 U mL^{-1}) with a platelet count at 3×10^8 mL^{-1}, and placed in a 37°C water bath for 30 min before use.

All procedures involving the collection of blood from mice were approved by the Institutional Animal Care and Use Committee (IACUC). The mouse was anesthetized with ketamine/xylazine mix during the terminal blood collection via inferior vena cava; anticoagulant (Clexane, 40 U mL^{-1}) was pre-loaded in syringe. After the blood collection (0.8-1 mL), a final concentration of 1X ACD buffer was added to the blood. Whole blood that was transferred to a small separation tube was centrifuged at 250 g for 2.5 min with soft brake. Platelet-rich plasma was obtained and centrifuged at 1950 g for 1 min. The platelet pellet was resuspended into platelet washing buffer pre-added with Clexane (20 U mL^{-1}) and apyrase (0.01 U mL^{-1}), then centrifuged again at 1950 g for 1 min. The platelet pellet was resuspended with Hepes-Tyrode buffer pre-added with apyrase (0.02 U mL^{-1}), and placed in a 37°C water bath for 30 min before use.

2.3 Mouse T Cell Collection

All procedures involving the collection of T cells from mice were approved by IACUC. T cell purification from mouse spleen was performed using the Stemcell kit, cat. # 19853. Briefly, the mouse was euthanized first with CO_2; spleen was collected into culture medium R10 (purchased RPMI 1640 1X w/L-glutamine, Corning 10-4-CM; adding 100 ml FBS, 10 ml P/S, 10 ml Hepes and 10 ml Sodium Pyruvate per 1 L). Spleen was then grinded with 3 ml R10 through a 70 um cell strainer placed on top of a 6-cm Petri dish using a 3 ml syringe plunger end, and RBCs lysed using the Mouse Erythrocyte Lysing Kit (#WL2000, R&D Systems). CD8 T cells were then negatively purified with Mouse CD8+ T Cell Enrichment Kit (cat#19853, Stemcell Technologies), following the EasySep protocol.

2.4 RBC and Glass Bead Preparation for BFP Experiments

8-10 μL of human blood was collected from finger prick and centrifuged to isolate RBCs. RBCs were biotinylated by incubating with Biotin-PEG3500-NHS (JenKem) solution [21] and partially swollen for BFP assembly by incubating with nystatin (Sigma-Aldrich).

The protocol of beads functionalization was described before [21]. Glass beads (Distrilab Particle Technology, Leusden, Netherlands) were first thiolated. To make OVA beads, the thiolated glass beads were incubated first with SA-MAL overnight, then with biotinylated OVA for 3 h. To make Fg and VWF-A1 beads, the protein was first mixed and incubated with MAL-PEG3500-NHS (JenKem) for 30 min [22,23]. The mixture was then incubated with the thiolated glass beads overnight. Beads were washed with and resuspended in phosphate buffer (27.6 g/L $NaH_2PO_4 \cdot H_2O$, 28.4 g/L Na_2HPO_4).

2.5 BFP Setups, Experiment Modes and Related Assays

BFP setup and operation has been described [21]. Briefly, in an experimental chamber filled with Hepes-Tyrode buffer (for platelet experiments) or L15 buffer (for T cell experiments), a biotinylated RBC was aspirated by a micropipette with a SA-coated probe bead attached to its apex, which altogether forms a force transducer (Fig. 1(A)). The bead was co-functionalized with proteins of interest to interact with the platelet aspirated by an opposing micropipette (Fig. 1(B)) driven by a piezoelectric translator (Physik Instrumente, Karlsruhe Germany). The horizontal position of the probe bead was tracked by a high-speed camera to signify the RBC axial deformation and, by calculation, the platelet-bead force. For force clamp experiments, the BFP spring constant k, determined using Evans' model [24], was set to 0.3 or 0.25 pN nm^{-1} for clamping forces higher or lower than 10 pN, respectively, by adjusting the aspirating pressure.

For force ramp experiments, k was set to 0.3 or 0.4 pN nm^{-1} for ramping rates lower or higher than 1000 pN s^{-1}, respectively. Experimental data were collected and analyzed by LabView (National Instrument, Austin, TX). Apyrase with a final concentration of 0.02 U mL^{-1} was added into the experimental chamber to chelate ADP released from the platelets.

2.5.1 Force-Clamp Mode and Bond Lifetime Assay

Force-clamp mode was used to measure single receptor-ligand bond lifetimes under a range of constant forces. The probe bead ligand coating density was adjusted to keep the adhesion infrequent (~20%) to satisfy the necessary condition for most of the adhesions (> 89%) to be single bond events [25]. The platelet was driven to contact and impinge the probe bead, and then retracted at 3 μm s^{-1}. If no adhesion occurs between the two surfaces, the force signal will return to zero during the retraction (Fig. 1(C)). When binding was detected during retraction, the target pipette was held at a pre-set distance to wait for bond dissociation, which then returned to the original position to start a new cycle (Fig. 1(D)). Lifetime was defined as the duration of the clamping phase before bond dissociation (Fig. 1(D)). Lifetime data were binned according to the clamp forces; the forces and lifetimes in each bin were then averaged to plot the lifetime *vs.* force curve.

2.5.2 Fitting Lifetime Distributions by Two-State Model

Within each clamp force bin, "survival frequency" was defined for each lifetime event as the fraction of lifetime events that lasted longer than it. The survival frequency was then plotted against lifetime, and fitted by a two-state model [8] that assumes superposition of two exponential decays in Eq. (1):

$$ln(Survival\ frequency) = ln\left(\omega_1 e^{-k_1 t} + \omega_2 e^{-k_2 t}\right) \quad (1)$$

in which t is the lifetime, and k_i and ω_i are respectively the off-rate and fraction of the ith state. The sum of the two fractions always equals 1.

The off-rate of each state as a function of force was then fitted to the Bell's equation [15] depicted in Eq. (2):

$$k_i(f) = k_{i0} e^{\frac{f}{f_{ai}}}, \quad i = 1,2 \quad (2)$$

in which k_{i0} is the zero-force off-rate of the ith state, f is force, and f_{ai} is defined as $f_{ai} = k_B T/a_i$ where a_i is the reactive compliance of the ith state, k_B is Boltzmann constant, and T is absolute temperature.

2.5.3 Force-Ramp Mode and Rupture Force Measurement

In a test cycle of force-ramp mode [25], the platelet approached and contacted the probe bead and retracted. A tensile force signal following retraction reports an adhesion event (Fig. 1(E)) between the platelet and the bead. The force loading rate was calculated based on the slope of the force-ramp phase, and the peak force right before bond dissociation was recorded as the rupture force (Fig. 1(E)).

2.5.4 Deriving Off-Rates by Fitting Rupture Force Distribution

The rupture force distribution under a constant loading rate can be used to calculate the effective off-rate (k_E) under different forces (f) using a previously described theoretical model which assumes no functional form of k_E against f [14]:

$$k_E(f) = \frac{r_f p_d(f)}{1 - P_c(f)} \quad (3)$$

where r_f is the force loading rate, and p_d and P_c are respectively the probability density and cumulative probability of the distribution.

If only one dissociation state exists for the receptor-ligand pair, the k_E equals the off-rate of this dissociation state. If two or more dissociation states co-exist, k_E equals the reciprocal of the average lifetime of all states.

2.5.5 Fitting Force-Ramp Off-Rates with an Upgraded State Transition Model

Evans' equation [17] first described a state transition model that describes how force shifts bonds to the dissociating state in the force-ramp assay, with the assumption of rapid inner conversion (at every moment, the transition of bonds between the two states rapid reaches equilibrium):

$$\begin{cases} \frac{dP}{dt} = \frac{d(S_1+S_2)}{dt} = -k_1 S_1 - k_2 S_2 \end{cases} \tag{4}$$

$$\begin{cases} \frac{S_1}{S_2} \approx \frac{k_{21}}{k_{12}} = e^{\frac{\Delta E_{21} - f\Delta x_{12}}{k_B T}} \end{cases} \tag{5}$$

where S_1 and S_2 are respectively the probability of bonds in State 1 (fast-dissociating) and 2 (slow-dissociating) surviving at time t (meaning not yet ruptured), and P is the probabilities of all bonds surviving at time t. k_B is the Boltzmann constant, T is temperature, and k_{12} and k_{21} are respectively the conversion rate from State 1 to State 2 and *vice versa*. ΔE_{21} is the energy difference between the two states at zero force, and Δx_{12} is the movement distance in the direction of force f when a bond transits from State 1 to State 2 (which explains why a tensile force shifts more bonds to State 2).

The above model only considers the impact of force magnitude to the bond state. To add force loading rate r_f as a second factor, a new function $U_{21}(r_f)$ (which equals zero when $r_f = 0$), the energy difference contributed by r_f, was added to Eq. (5):

$$\frac{S_1}{S_2} \approx \frac{k_{21}}{k_{12}} = e^{[\Delta E_{21} - f\Delta x_{12} + U_{21}(r_f)]/k_B T} \tag{6}$$

Combing Eqs. (4) and (6), we have:

$$\begin{cases} -\frac{\frac{dP}{dt}}{P} = \frac{k_1 Z(r_f) + k_2 e^{f/f_{12}}}{Z(r_f) + e^{f/f_{12}}} \\ Z(r_f) = e^{[\Delta E_{21} + U_{21}(r_f)]/k_B T} \end{cases} \tag{7}$$

in which $f_{12} = k_B T / \Delta x_{12}$. The expression equations of k_1 and k_2 as a function of force have already been derived from force-clamp assay (Fig. 2(C)), and $-\frac{\frac{dP}{dt}}{P} = -\frac{r_f \frac{dP}{df}}{P} = \frac{r_f p_d}{1-P_c}$ is in fact the effective off-rate k_E (Eq. (3)).

Fitting GPIbα–A1 force-ramp "k_E vs. force" data under different force loading rates to Eq. (7) (Fig. 3(D)) derives $f_{12} = k_B T/\Delta x_{12} = 16.3$ pN and ($\Delta E_{21} + U_{21}$) as a function of r_f (Fig. 3(E), *black open circles*).

2.6 Statistical Analysis

Statistical significance was assessed by two-tailed Student's *t*-test.

3 Results

3.1 Deriving Two Dissociation States from Directly Measured Platelet GPIbα-VWF-A1 Lifetimes

Platelet tethering via GPIbα binding to VWF-A1 initiates both hemostasis and thrombosis under high shear stress [26] in the arteries and arterioles. To examine the binding kinetics that governs the physiological and pathological platelet functions, we performed the BFP experiments to measure this interaction under controlled tensile force. Briefly, the VWF-A1 domain and streptavidin were co-immobilized on a glass bead (Figs. 1(A), 1(B)), which was then attached to the apex of a micropipette-aspirated biotinylated red blood cell (RBC). On the opposing side, a micropipette-aspirated human

platelet was driven by a piezo to repeated touch the bead and retract, allowing adhesion events to happen in a stochastic manner (Figs. 1(A), 1(B)). Force was determined by the RBC deformation, which was monitored in real-time (Methods). Upon the retraction of the platelet, force returning to zero would indicate no adhesion (Fig. 1(C)), whereas a tensile force would signify an adhesion event (Fig. 1D). As a control, the addition of an VWF-A1 blocking antibody 6G1 [27] eliminated most of the adhesion events (Fig. 2(A)), confirming the binding specificity.

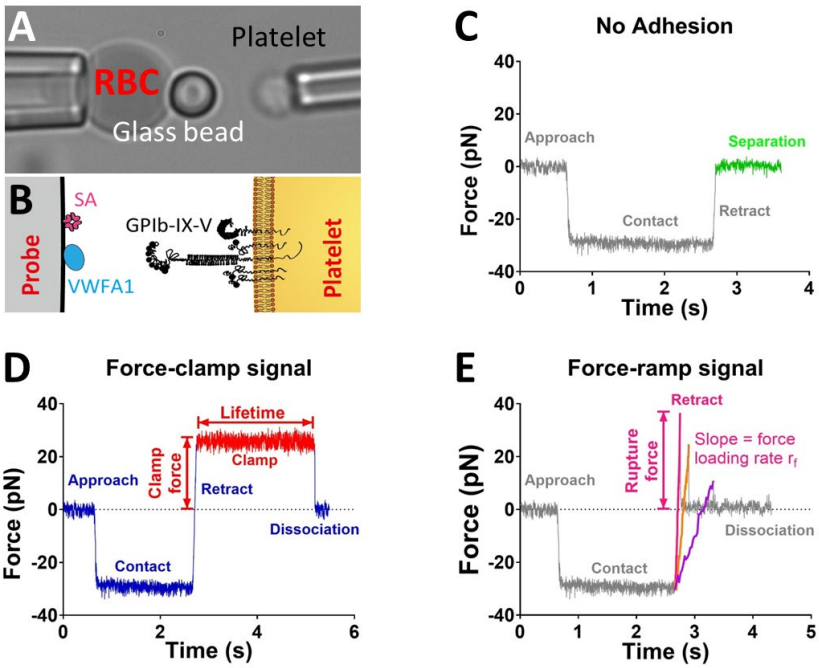

Figure 1: BFP setup for force-clamp and force-ramp assays. (**A**) A micrograph of BFP setup showing a human platelet aligned with an aspirated RBC-based force probe. A ligand-coated glass bead is placed on the RBC apex for biological functionalization. (**B**) Illustration of the molecular system of interest. On the probe side, the bead is coated with VWF-A1 domain, which is a ligand for platelet GPIbα. (**C**) "Force *vs.* time" trace of a representative BFP cycle with no adhesion. (**D**) "Force *vs.* time" trace of a representative force-clamp cycle with a lifetime event. The clamp force and lifetime duration are annotated. (**E**) Superimposed "force *vs.* time" traces of three representative force-ramp cycles with different force loading rates (colored in magenta, orange and purple respectively). Rupture force is annotated for one representative signal curve

To directly measure bond lifetimes, the VWF-A1 coating density was titrated to achieve ~ 20% adhesion frequency, so that most (> 89%) adhesion events were mediated by single GPIbα-A1 bonds [25]. By clamping the bond and waiting for its dissociation, lifetimes were collected under different clamp forces (Fig. 1(D)). The "lifetime vs. force" manifested a tri-phasic "slip-catch-slip" pattern agreeing with previous studies [23,28]: the average lifetime first decreased with incrementing force when force is < 15 pN, but increased with force in the range of 15-25 pN with a peak value of ~ 2.5 s, beyond which it decreased again (Fig. 2(B)).

Based on Bell's equation [15], the off-rate (reciprocal of lifetime) of a receptor-ligand bond should increase exponentially with force if the bond only adopts a single dissociating state; accordingly, its lifetime curve exponentially decays with force. The 'catch' behavior in the GPIbα-A1 lifetime curve suggested that the sampled single bonds were a mixture of at least two subpopulations in terms of dissociation state, and the fractions of the subpopulations shifted with force magnitude [8,23]. In order to delineate these dissociation states, we adopted a biophysical model that assumes the superposition of two

states (fast- and slow-dissociating; Methods) [23], which fitted well with the experimental data ($R^2 \geq 0.8$ under all forces). The calculated off-rates of the slow-dissociating state (k_2) were approximately one order of magnitude less than those of the fast-dissociating state (k_1) under all forces, while the fraction of the slow-dissociating subpopulation (ω_2) gradually increased with force, agreeing with the catch bond behavior and indicating a force-induced bond activation (Figs. 2(C), 2(D)). Importantly, the off-rates of both bond states respectively fitted nicely to Bell's equation, demonstrating that both states followed the first-order dissociation kinetics [8] (Fig. 2(C), fitting parameters annotated).

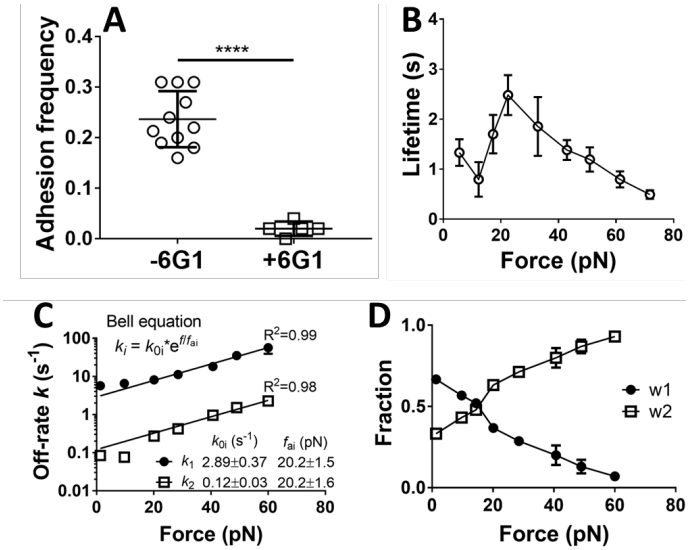

Figure 2: Human platelet GPIbα-A1 lifetime measurements and two-state analysis. (**A**) GPIbα-A1 adhesion frequency (points and mean ± s.d.) in the absence and presence of VWF-A1 blocking antibody 6G1, which eliminated most of the adhesion and confirmed binding specificity. **** $p < 0.0001$, assessed by unpaired, two-tailed Student's *t*-test. (**B**) Mean ± s.e.m., "lifetime *vs.* force" curve of GPIbα-A1 manifests a tri-phasic "slip-catch-slip" pattern. (**C**) Mean ± s.e.m., off-rates of fast- (k_1) and slow-dissociating (k_2) states under different forces, calculated by fitting the lifetime data to the two-state model (Methods). The "off-rate *vs.* force" curve are respectively fitted to Bell equation (equation and derived parameters all annotated in the graph) with R^2 denoted. (**D**) Mean ± s.e.m., fractions of the fast- (w_1) and slow-dissociating (w_2) bonds under different forces

3.2 Force Loading Disrupts Bond Stability

To investigate whether the force-ramp off-rates can predict force-clamp lifetime results, the BFP was set to pull each bond with a pre-set loading rate until the bond was ruptured (Fig. 1(E); Methods). The rupture force data were collected under a wide range of force loading rates (Fig. 3(A)), and segregated based on the loading rate to acquire distribution histograms (Fig. 3(B)) [14,29]. The distributions were then fitted to derive the effective off-rates (k_E) (Methods).

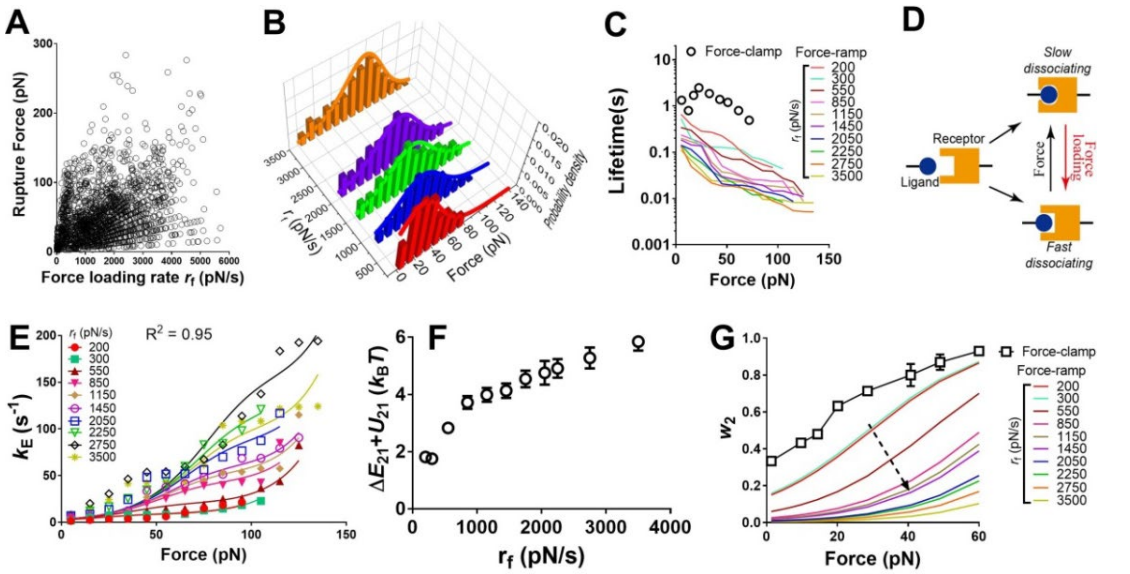

Figure 3: Discrepancies between force-ramp and -clamp off-rates reconciled by an upgraded state transition model. (**A**) Scatter plot of "rupture force *vs.* force loading rate r_f" (2047 points in total). (**B**) Representative histograms of rupture force distributions (> 100 measurements for each r_f bin) at various force loading rates. The upgraded state transition model was used to back-calculate the distribution (*curves*), which fit well with the data. (**C**) "$1/k_E$ (lifetime) *vs.* force" relations (*colored curves*) were estimated from individual rupture force histograms according to Eq. (3), which were plotted in semi-log scale together with the lifetime curve measured by force-clamp assay (duplicated from Fig. 2(B); *black circles*). (**D**) Illustration of the upgraded state transition model. The receptor–ligand pair can form a bond in two possible states: fast- or slow-dissociating. Force induces the transition of the bond from fast- to slow-dissociating state, whereas force loading conversely shifts bonds from the slow-dissociating state to the fast-dissociating state. (**E**) "k_E (effective off-rate) *vs.* force" relations (*points*) under 10 different r_f (calculated from panel C) were simultaneously fitted to the upgraded state transition model (Eq. (7); Metahods) using shared parameters (*curves*); R^2 denoted. (**F**) Mean ± standard error, "($\Delta E_{21} + U_{21}$) vs. r_f" relation derived from fitting curves in panel (E) to the upgraded state transition model. (G) Fraction of bonds in the slow-dissociating state (w_2) under different force (*colored curves*) showed a clear negative correlation with the force loading rate (*black arrow*). The w_2 calculated form force-clamp assay (duplicated from Fig. 2(D); *black squares*) was also plotted

Intriguingly, the derived lifetime ($1/k_E$) curves manifested a slip-bond behavior under all force loading rates (Fig. 3(C), *curves*) and were generally lower than the tri-phasic lifetime curve directly measured from the force-clamp assay (Fig. 3(C), *open circles*). Moreover, the average lifetimes across forces became shorter as loading rate increased (Fig. 3(C)). Considering that the force-clamp assay holds the bond still with $r_f = 0$, these results indicated that the molecular interaction was disrupted by force loading in a rate-dependent fashion. Notably, a similar phenomenon has previously been observed in P-selectin-sPSGL-1 and P-selectin-G1 interactions [14].

3.3 Reconciling the Off-Rate Discrepancy Using an Upgraded State Transition Model

Force can activate bonds by decreasing the energy of the slow-dissociating state relative to the fast-dissociating state, thereby transiting bonds from fast- to slow-dissociating state, which underlies the 'catch bond' behavior [8,17] (Fig. 2(D)). We hypothesize that force loading may affect bond dissociation by conversely shifting more bonds to the fast-dissociating state (Fig. 3(D)). A biophysical model was previously created to describe the transition of bonds between dissociation states [17], which only considered the effect of force magnitude. Here, we introduced a new parameter, $U_{21}(r_f)$, to depict the

energy difference between the two dissociation states contributed by force loading rate r_f (Methods; Eq. (7)). A higher U_{21} value indicates an increase of the energy level of the slow-dissociating state relative to the fast-dissociating state, which should drive bonds to transition to the more stable, fast-dissociating state.

Our new model fitted nicely with the "k_E *vs.* force" data under all force loading rates (Fig. 3(E)). Importantly, the derived values of ($\Delta E_{21} + U_{21}$) manifested an obvious positive trend against r_f (Fig. 3(F); ΔE_{21} is a constant that represents the default energy difference between two states in the absence of force and force loading), which agreed with our hypothesis. The fractions of slow-dissociating bonds (w_2) were then calculated, which demonstrated a concurrent regulation by both force magnitude and loading rate that counteracted with each other (Fig. 3(G)). Under the same force, the fractions of slow-dissociating bonds in force-ramp were all lower than those in the force-clamp condition, and exhibited a negative correlation to r_f, confirming the bond state transitioning triggered by force loading (Fig. 3(G)). By using the derived parameters to back-calculate the rupture force distributions, we found that the model could predict our experimental data acquired under all force loading rates (Fig. 3(B), *curves*). Overall, these results demonstrated the robustness of our new state transition model.

3.4 Force Loading Shifts Bonds to Fast-Dissociating State in Two Mouse Molecular Systems

To test if the model is also applicable to other molecular systems, we investigated the bond dissociation in mouse T cell receptor (TCR)-OVA peptide:MHC and mouse platelet integrin $\alpha_{IIb}\beta_3$-fibrinogen (Fg). The former interaction initiates T cell activation in adaptive immune responses [4,30], while the latter plays a key role in platelet aggregation and thrombus growth [26]. Both interactions manifested a catch bond in force-clamp assay [4], indicating the mixture of two dissociation states. In contrast, the force-ramp assay yielded a slip bond with generally shorter lifetimes, similar to that of the GPIbα-VWF-A1 binding (Fig. 4(A)), suggesting that force loading takes effect again. However, these lifetimes did not show a correlation with r_f (Fig. 4(A), *curves*); accordingly, the derived k_E under different r_f also overlapped with one another (Fig. 4(B), *points*), which suggested insensitivity of bond stability to force loading rate [6,16].

To understand these seemingly contradicting results, we considered the possibility that in these two systems the effect of force loading was so strong that even the lowest r_f used (250 pN/s for $\alpha_{IIb}\beta_3$-Fg and 150 pN/s for TCR-OVA) already transited all of the bonds to the fast-dissociating state (i.e., none in the slow-dissociation state). To test this hypothesis, force-clamp lifetimes were used to derive the parameters of fast- and slow-dissociating states in the two systems (Figs. 4(C), 4(D)). Remarkably, the calculated fast-dissociating state off-rates of both systems (Fig. 4(B), *solid curves*) aligned well with their corresponding force-ramp k_E data (Fig. 4(B), *points*) under all forces, suggesting that the bonds in the force-ramp assay were indeed all in the fast-dissociating state. In the context of the new state transition model, the results suggested that the U_{21} of these two molecular systems increased steeply with r_f, so that a relatively small r_f already resulted in a very large U_{21}. To study the "U_{21} *vs.* r_f" relation in these two molecular systems would require other DFS techniques, e.g., the optical tweezer [31], that have a much softer force transducer than that of BFP to achieve much slower force loading.

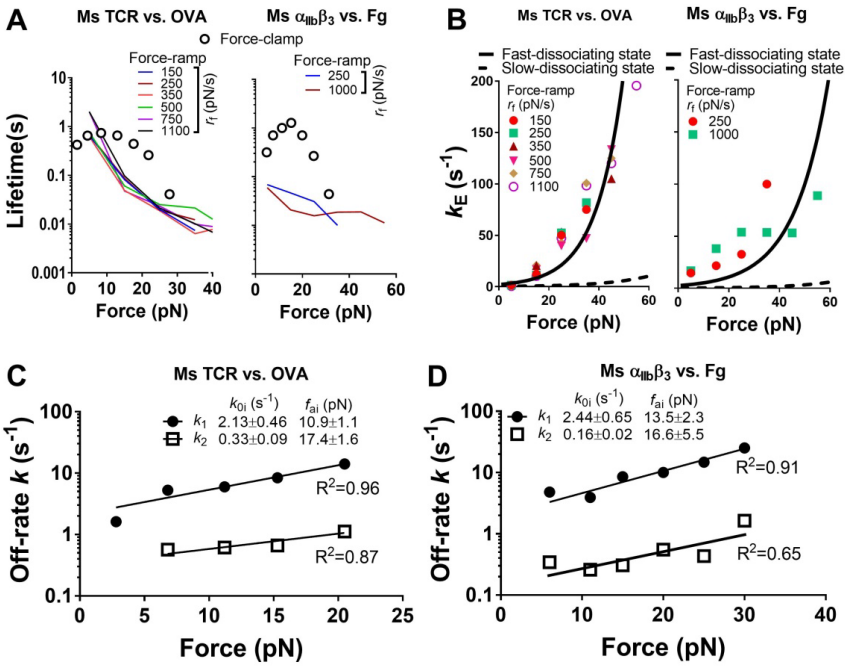

Figure 4: Investigating the bond stability of mouse TCR *vs.* OVA and mouse platelet integrin $\alpha_{IIb}\beta_3$ *vs.* fibrinogen (Fg) systems. (**A**) "$1/k_E$ (lifetime) *vs.* force" relations (*colored curves*) of mouse TCR-OVA (*left*) and $\alpha_{IIb}\beta_3$-Fg (*right*) interactions estimated from force-ramp assay, which were superimposed with the force-clamp lifetime curves (*black circles*). (**B**) "k_E *vs.* force" relations (*points*) of mouse TCR *vs.* OVA (*left*) and $\alpha_{IIb}\beta_3$ *vs.* Fg (*right*) under different r_f (calculated from panel A). Black curves represent the off-rates of the fast-dissociating (*solid curve*) and slow-dissociating (*dotted curve*) states calculated from the force-clamp lifetimes (panels C and D). (**C**,**D**) Mean ± s.e.m., off-rates of fast- (k_1) and slow-dissociating (k_2) states of mouse TCR *vs.* OVA (C) and $\alpha_{IIb}\beta_3$ *vs.* Fg (D) interactions under different forces, calculated by fitting the force-clamp lifetime data to the two-state model (Methods). The "off-rate *vs.* force" curve are respectively fitted to Bell equation (equation and derived parameters all annotated in the graph) with R^2 denoted

4 Discussion

In this work, we defined the role of force loading rate in regulating molecular binding kinetics. The newly developed model provided a theoretical foundation for using different DFS assays in combination to comprehensively characterize molecular binding.

The off-rate discrepancy between force-clamp and force-ramp assays was first reported in early 2000s when single-molecule DFS technologies started to prevail [5,18]. Meanwhile, some force-ramp assays noticed that the average rupture force of molecular bonds can be independent to or even negatively correlated with r_f, which cannot be explained by models assuming that k_{off} is only a function of force [20,22]. By performing AFM experiments, a study on purified P-selectin [14] demonstrated that k_{off} is affected by how force is applied over time, denoted as "force history." Here, we identified force loading rate as the dominating factor in force history and showed that fast force loading disrupts the bond stability by transiting bonds into the fast-dissociating state. By incorporating an energy parameter associated with force loading rate, we established a new bond dissociation model which reconciled the unsolved off-rate discrepancy between the two mainstream DFS assays. Notably, this disruptive effect of force loading should be distinguished from another "force history" effect specific to P-selectin-PSGL-1 interaction [32], where fast force loading activates, instead of inactivates, the bond via a "sliding-rebinding mechanism". This effect is also to be distinguished from the reinforcement of stem cell integrin binding over a threshold loading rate, which requires myosin-dependent stiffness sensing and mechano-signaling of the cell [33].

The biophysics underlying how force loading changes the energy difference between the two dissociation states still remains elusive. We postulate that the force-induced bond activation is a "maturation process" that requires time; fast force loading may rupture the bonds before state transition takes place, thereby locking the bonds in the fast-dissociating state. Obviously, the disruptive effect of force loading does not occur ubiquitously: under circumstances where the molecular interaction only adopts a single dissociation state [34], the off-rates derived from force-clamp and force-ramp assays should be in agreement. It should also be noted that the state transition model established here is only applicable to systems with two dissociation states. In the cases where three or more states co-exist [8], a more complicated theory would be required.

In physiological contexts, the mechanical environment experienced by cells is highly dynamic and complex. DFS allows the observation of one bond at a time while precisely controlling the force waveform [35] on the bond, which is advantageous for mechanistic studies. However, the applied forces on cells are "simplified", and such simplification may affect the binding kinetics, as exemplified by the off-rate discrepancies between DFS assays. The force waveform affects cell mechano-signaling as well, as exemplified by the physiological and pathological cyclic stretch which differentially regulated glucocorticoid receptor nuclear translocation and mitochondrial remodeling in endothelial cells [36,37]. Also, in DFS experiments it has been observed that platelet GPIb and T cell surface TCR can only initiate intracellular calcium signaling following sustained, but not quickly ruptured, ligand binding [3,4]. Therefore, better characterization of cell adhesion and mechano-signaling requires the appropriate selection of DFS assays to mimic the mechanical stimulations cells physiologically experience while interacting with their environment. For instance, platelets and neutrophils adhered to the vascular wall experience nearly constant shear force from the bloodstream [38], and therefore it is more reasonable to select the DFS force-clamp assay to study their adhesion and mechano-signaling [3]. In contrast, platelets aggregating in disturbed blood flow [2,39] and cells forming focal adhesions on a substrate [40,41,42] are subjected to highly dynamic forces, which can be better recapitulated by the force-ramp assay.

Acknowledgements: We thank Z. Ruggeri (The Scripps Research Institute), B. Petrich (Emory University) for providing precious reagents, and Y. Sakurai, D. Myer, Y. Qiu and R. Tran from W. Lam lab (Georgia Tech) for the blood collection.

This work was supported by grants from the NIH (HL1320194-C.Z.) and the Cardiac Society of Australia and New Zealand BAYER Young Investigator Research Grant (L.A.J.). Y.C. is a MERU (Medolago-Ruggeri) Foundation post-doctoral awardee. L.A.J. is an Australian Research Council DECRA Fellow (DE190100609) and a former National Heart Foundation of Australia postdoctoral fellow (101798).

Author contributions: Y.C. designed and performed experiments, established the biophysical model, analyzed data and wrote the paper; J.L. performed experiments, analyzed data and wrote the paper; K.L, Z.Y., B.L. and L.A.J. performed experiments and analyzed data; C.Z. supervised the study, designed experiments, provided guidance on the biophysical model and wrote the paper. Research activities related to this work were complied with relevant ethical regulations.

Competing Financial Interests: The authors have no conflict of interest to declare.

References

1. Su QP, Ju LA. Biophysical nanotools for single-molecule dynamics. *Biophysical Reviews* **2018**, 10(5): 1349-1357.
2. Chen Y, Ju L., Zhou F., Liao J., Xue L et al. An integrin αIIbβ3 intermediate affinity state mediates biomechanical platelet aggregation. *Nature Materials* **2019**, 18(7): 760-769.
3. Ju L, Chen Y, Xue L, Du X, Zhu C. Cooperative unfolding of distinctive mechanoreceptor domains transduces force into signals. *eLife* **2016**, 5: e15447.

4. Liu B, Chen W, Evavold BD, Zhu C. Accumulation of dynamic catch bonds between TCR and agonist peptide-MHC triggers T cell signaling. *Cell* **2014**, 157(2): 357-368.
5. Marshall BT, Long M, Piper JW, Yago T, McEver RP et al. Direct observation of catch bonds involving cell-adhesion molecules. *Nature* **2003**, 423(6936): 190-193.
6. Evans E. Probing the relation between force-lifetime-and chemistry in single molecular bonds. *Annual Review of Biophysics and Biomolecular Structure* **2001**, 30(1): 105-128.
7. Hanley W, McCarty O, Jadhav S, Tseng Y, Wirtz D et al. Single molecule characterization of P-selectin/ligand binding. *Journal of Biological Chemistry* **2003**, 278(12): 10556-10561.
8. Chen W, Lou J, Zhu C. Forcing switch from short- to intermediate- and long-lived states of the alphaA domain generates LFA-1/ICAM-1 catch bonds. *Journal of Biological Chemistry* **2010**, 285(46): 35967-35978.
9. Choi YI, Duke-Cohan JS, Chen W, Liu B, Rossy J et al. Dynamic control of beta1 integrin adhesion by the plexinD1-sema3E axis. *Proceedings of the National Academy of Sciences of the United States of America* **2014**, 111(1): 379-384.
10. Kong F, Garcia AJ, Mould AP, Humphries MJ, Zhu, C. Demonstration of catch bonds between an integrin and its ligand. *Journal of Cell Biology* **2009**, 185(7): 1275-1284.
11. Li F, Redick SD, Erickson HP, Moy VT. Force measurements of the alpha5beta1 integrin-fibronectin interaction. *Biophysical Journal* **2003**, 84(2 Pt 1): 1252-1262.
12. Wojcikiewicz EP, Abdulreda MH, Zhang X, Moy VT. Force spectroscopy of LFA-1 and its ligands, ICAM-1 and ICAM-2. *Biomacromolecules* **2006**, 7(11): 3188-3195.
13. Zhang X, Craig SE, Kirby H, Humphries MJ, Moy VT. Molecular basis for the dynamic strength of the integrin alpha4beta1/VCAM-1 interaction. *Biophysical Journal* **2004**, 87(5): 3470-3478.
14. Marshall BT, Sarangapani KK, Lou J, McEver RP, Zhu C. Force history dependence of receptor-ligand dissociation. *Biophysical Journal* **2005**, 88(2): 1458-1466.
15. Bell G I. Models for the specific adhesion of cells to cells. *Science* **1978**, 200(4342): 618-627.
16. Evans E, Leung A, Hammer D, Simon, S. Chemically distinct transition states govern rapid dissociation of single L-selectin bonds under force. *Proceedings of the National Academy of Sciences of the United States of America* **2001**, 98(7): 3784-3789.
17. Evans E, Leung A, Heinrich V, Zhu, C. Mechanical switching and coupling between two dissociation pathways in a P-selectin adhesion bond. *Proceedings of the National Academy of Sciences of the United States of America* **2004**, 101(31): 11281-11286.
18. Hummer G, Szabo A. Kinetics from nonequilibrium single-molecule pulling experiments. *Biophysical Journal* **2003**, 85(1): 5-15.
19. Zhu C. Kinetics and mechanics of cell adhesion. *Journal of Biomechanics* **2000**, 33(1): 23-33.
20. Ruggeri ZM, Orje JN, Habermann R, Federici AB, Reininger AJ. Activation-independent platelet adhesion and aggregation under elevated shear stress. *Blood* **2006**, 108(6): 1903-1910.
21. Chen Y, Liu B, Ju L, Hong J, Ji Q et al. Fluorescence biomembrane force probe: concurrent quantitation of receptor-ligand kinetics and binding-induced intracellular signaling on a single cell. *Journal of Visualized Experiments* **2015**, (102): e52975.
22. Butera D, Passam F, Ju L, Cook KM, Woon H et al. Autoregulation of von Willebrand factor function by a disulfide bond switch. *Science Advances* **2018**, 4(2): 1477.
23. Ju L, Dong JF, Cruz MA, Zhu C. The N-terminal flanking region of the A1 domain regulates the force-dependent binding of von Willebrand factor to platelet glycoprotein Ibα. *Journal of Biological Chemistry* **2013**, 288(45): 32289-32301.
24. Ju L, Zhu C. Benchmarks of biomembrane force probe spring constant models. *Biophysical Journal* **2017**, 113(12): 2842-2845.
25. Chesla SE, Selvaraj P, Zhu, C. Measuring two-dimensional receptor-ligand binding kinetics by micropipette. *Biophysical Journal* **1998**, 75(3): 1553-1572.
26. Jackson SP. Arterial thrombosis-insidious, unpredictable and deadly. *Nature Medicine* **2011**, 17(11): 1423-1436.
27. Romo GM, Dong JF, Schade AJ, Gardiner EE, Kansas GS et al. The glycoprotein Ib-IX-V complex is a platelet counterreceptor for P-selectin. *Journal of Experimental Medicine* **1999**, 190(6): 803-814.

28. Ju L, Chen Y, Zhou F, Lu H, Cruz MA et al. Von Willebrand factor-A1 domain binds platelet glycoprotein Ibalpha in multiple states with distinctive force-dependent dissociation kinetics. *Thrombosis Research* **2015**, 136(3): 606-612.
29. Merkel R, Nassoy P, Leung A, Ritchie K, Evans E. Energy landscapes of receptor-ligand bonds explored with dynamic force spectroscopy. *Nature* **1999**, 397(6714): 50-53.
30. Smith-Garvin JE, Koretzky GA, Jordan MS. T cell activation. *Annual Review of Immunology* **2009**, 27: 591-619.
31. Friese ME, Rubinsztein-Dunlop H, Heckenberg NR, Dearden EW. Determination of the force constant of a single-beam gradient trap by measurement of backscattered light. *Applied Optics* **1996**, 35(6): 7112-7116.
32. Sarangapani KK, Qian J, Chen W, Zarnitsyna VI, Mehta P et al. Regulation of catch bonds by rate of force application. *Journal of Biological Chemistry* **2011**, 286(37): 32749-32761.
33. Jiang L, Sun Z, Chen X, Li J, Xu Y et al. Cells sensing mechanical cues: stiffness influences the lifetime of cell-extracellular matrix interactions by affecting the loading rate. *Acs Nano* **2016**, 10(1): 207-217.
34. Evans EA, Calderwood DA. Forces and bond dynamics in cell adhesion. *Science* **2007**, 316(5828): 1148-1153.
35. Chen Y, Li Z, Ju L. Tensile and compressive force regulation on cell mechanosensing. *Biophysical Reviews* **2019**, 11(3): 311-318.
36. Baba M, Shinmura A, Tada S, Amo T, Tsukamoto A. Mitochondrial remodeling in endothelial cells under cyclic stretch is independent of Drp1 activation. *Molecular & Cellular Biomechanics* **2019**, 16(1): 1-12.
37. Nayebosadri A, Ji JY. Lamin A/C regulates endothelial glucocorticoid receptor nuclear translocation in response to cyclic stretch. *Molecular & Cellular Biomechanics* **2016**, 13(1): 57-85.
38. McEver RP, Zhu C. Rolling cell adhesion. *Annual Review of Cell and Developmental Biology* **2010**, 26: 363-396.
39. Nesbitt WS, Westein E, Tovar-Lopez FJ, Tolouei E, Mitchell A et al. A shear gradient-dependent platelet aggregation mechanism drives thrombus formation. *Nature Medicine* **2009**, 15(6): 665-673.
40. Galior K, Liu Y, Yehl K, Vivek S, Salaita K. Titin-based nanoparticle tension sensors map high-magnitude integrin forces within focal adhesions. *Nano Letters* **2016**, 16(1): 341-348.
41. Zhang Y, Ge C, Zhu C, Salaita K. DNA-based digital tension probes reveal integrin forces during early cell adhesion. *Nature Communications* **2014**, 5: 5167.
42. Zhang Y, Qiu Y, Blanchard AT, Chang Y, Brockman JM et al. Platelet integrins exhibit anisotropic mechanosensing and harness piconewton forces to mediate platelet aggregation. *Proceedings of the National Academy of Sciences of the United States of America* **2018**, 115(2): 325-330.